Automatic Generation of Anatomic Characteristics from Cerebral Aneurysm Surface Models

M. Neugebauer[1], K. Lawonn[1], O. Beuing[2], B. Preim[1]

[1]*Department of Simulation and Graphics, University of Magdeburg, Germany*

[2]*Department of Neuroradiology, University Hospital Magdeburg, Germany*

Address: Universitätsplatz 2, 39106 Magdeburg, Germany, Tel.: +49 391 67 12759,

Fax: +49 391 67 11164, Mail: mathias.neugebauer@ovgu.de

Keywords: Cerebral Aneurysm, Decomposition, Automatic Characterization, Anatomic Descriptors

Abstract - PURPOSE: Computer-aided research on cerebral aneurysms often depends on a polygonal mesh representation of the vessel lumen. To support a differentiated, anatomy-aware analysis, it is necessary to derive anatomic descriptors from the surface model. We present an approach on automatic decomposition of the adjacent vessels into near- and far-vessel regions and computation of the axial plane. We also exemplarily present two applications of the geometric descriptors: automatic computation of a unique vessel order and automatic viewpoint selection. METHODS: Approximation methods are employed to analyze vessel cross-sections and the vessel area profile along the centerline. The resulting transition zones between near- and far vessel regions are used as input for an optimization process to compute the axial plane. The unique vessel order is defined via projection into the plane space of the axial plane. The viewing direction for the automatic viewpoint selection is derived from the normal vector of the axial plane. RESULTS: The approach was successfully applied to representative datasets exhibiting a broad variability with respect to the configuration of their adjacent vessels. A robustness analysis showed that the automatic decomposition is stable against noise. A survey with 4 medical experts showed a broad agreement with the automatically defined transition zones. CONCLUSION: Due to the general nature of the underlying algorithms, this approach is applicable to most of the likely aneurysm configurations in the cerebral vasculature. Additional geometric information obtained during automatic decomposition can support correction in case the automatic approach fails. The resulting descriptors can be used for various applications in the field of visualization, exploration and analysis of cerebral aneurysms.

Introduction

In the clinical routine geometric analysis of cerebral aneurysms is mainly performed on image data, directly obtained from the scanning device. 2D measurement tools, like a virtual ruler, applied to contrast enhanced 2D-DSA

images, are commonly used to determine parameters like the aneurysm size or neck-to-dome ratio [1]. In some cases an unobstructed 2D-view on the side of the aneurysm cannot be gained, due to positioning limitations of the scanning device or because the aneurysm is occluded by surrounding vessels. In such cases clipping planes are applied to a direct 3D-volume-rendering of the vessels and 3D tools are used for quantification. Even though the working domain is 3D, it is still directly derived from the image data. However, computer-aided biomedical research related to the morphology and hemodynamics of aneurysms makes it necessary to explicitly represent the vessel lumen by means of a polygonal mesh. For example, CFD-based blood flow simulations are becoming increasingly important, since geometric descriptors like shape, size and location of the aneurysms are not sufficient to understand the aneurysm formation and to estimate the risk of rupture [2]. Current medical research incorporates flow data to optimize or develop new intravascular treatment options [3] while the EU-funded project THROMBUS (European FP7-ICT project no. 269966) develops new methods for thrombosis modelling based on flow simulations.

However, geometric analysis, although performed on the polygonal meshes rather than on the underlying image data, still plays an important role. For instance, the software system GIMIAS [4], developed in the course of the international aneurysm research project @NEURIST, provides a toolset for geometric quantification of polygonal vessel meshes in the context of flow analysis. It provides measurement tools (distances, areas and volume), which are comparable to their image-based counterparts, but also tools for decomposing the polygonal vessel mesh. The decomposition of the polygonal mesh into aneurysm sac and adjacent vessels allows for a differentiated exploration of the flow data. For instance, after decomposition, the turbulence behaviour of flow in the aneurysm and the adjacent vessels can be compared, in order to understand how vessel implants (e.g. stent) influence the thrombosis within the aneurysm.

Several approaches exist to decompose the mesh into an aneurysm sac region and an adjacent vessels region without further differentiation. However, recent work on flow cluster analysis [5] implies that an additional decomposition of the adjacent vessels can further improve the analysis process. It has shown that flow in adjacent vessels exhibit complex turbulence close the aneurysm, compared to flow further away from the aneurysm.

A decomposition of the adjacent vessels can not only support flow analysis, but can also provide additional geometric descriptors for abstract dataset description and interaction with the datasets.

We present an automatic approach for decomposition of the adjacent vessels into near- and far-vessel regions. We further apply the decomposition to compute a characteristic axial plane. This plane is useful for multiple purposes, of which we present two: the definition of a unique vessel order of the adjacent vessels, which can enhance dataset descriptions when organizing research databases, and computation of an optimal initial position of the virtual camera (viewpoint selection), which supports interaction with the 3D visualization of surface and/or flow data.

Related Work

For geometric quantification and analysis of polygonal vessel meshes, the Vascular Modelling Toolkit (VMTK) of Antiga et. al. provides a broad set of tools, e.g. for centerline extraction or bifurcation characterization [6]. This toolkit was also applied to cerebral aneurysms [7] in order to calculate specific geometric descriptors like the angle between adjacent vessels and the aneurysm neck. A common approach to aid vessel analysis is to decompose the anatomy into aneurysm sac and adjacent vessels. Such a decomposition is used for geometry based analysis and calculation of shape indices of the aneurysm sac [8]. Other approaches concentrate on the extraction of the aneurysm neck [9] or the ostium [10]. As discussed in [11], the morphology of the vessel has major impact on flow characteristics, like velocity or turbulence. Thus, including geometric information of the extracted anatomic features (neck, ostium, etc.) into the analysis process helps to investigate specific segments of the flow field or is used to extract certain flow features. Examples are the analysis of time-dependent flow characteristics at the ostium [12] or the investigation how the shape and angle of the inflow jet relates to the risk of rupture [13]. Our automatic approach on decomposing the adjacent vessels into near- and far-vessel regions introduces additional geometric descriptors. These can be used for a finer distinction of functionally relevant flow field segments.

Methods

As the exploration of intra-aneurysmal flow for risk analysis and development of new treatment options is not part of the common clinical procedure, a decomposition method to aid this process is a tool for medical research. However, a clinical usage is possible, as soon a flow data becomes available in clinical routine. The decomposition should be automatic for two reasons: to yield reproducible results and to avoid tedious interaction, since the medical researcher has to handle interactions with multiple degrees of freedom on multi-dimensional data when using established exploration software (e.g. EnSight). Geometric descriptors derived from the decomposition should not only aid the analysis process but also support the interaction with the data.

In the following, we present the data-driven workflow of our decomposition approach. A polygonal vessel mesh is reconstructed from image data. The aneurysm ostium, which separates aneurysm sac and adjacent vessels, and the adjacent vessel centerlines are determined. These geometric descriptors and the polygonal vessel mesh form the input for the automatic vessel analysis, based on approximation methods. The results of the analysis are *transition zones* that separate the near-vessel region from the far-vessel regions. From this decomposition, the *axial plane*, another geometric descriptor, is derived. We present two applications for this multi-purpose plane: automatic definition of a vessel order and the support of 3D-interaction by calculating a good initial position for the virtual camera. Figure 1 shows an overview of the data-driven workflow.
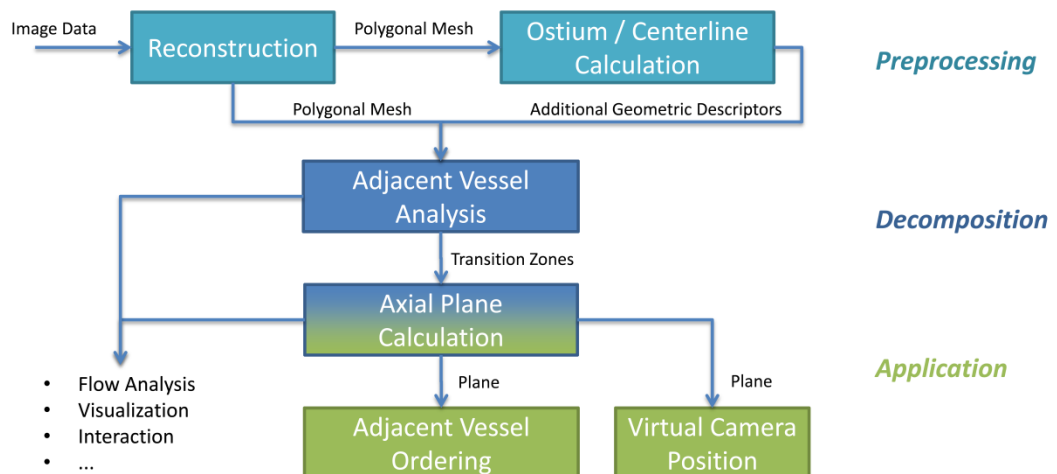
Fig. 1 *The data driven-workflow: polygonal surface mesh, ostium and centerlines are input for the decomposition, the resulting transition zones are used for the axial plane calculation and two example applications*

Before we describe the workflow steps in greater detail, we give a short definition of near- and far-vessel region and the axial plane.

Definition of Near-/Far-Vessel Region and Axial Plane

Cerebral aneurysms exhibit broad shape variability. This concerns the size and shape of the aneurysm sac (e.g. presence of satellites or local surface curvature) as well as the overall vessel configuration, e.g. the number of inflow and outflow vessel segments, the diameter of the adjacent vessels and the orientation of the aneurysm with respect to the vessels. However, on a more abstract level, all aneurysms exhibit the same basic geometric layout.
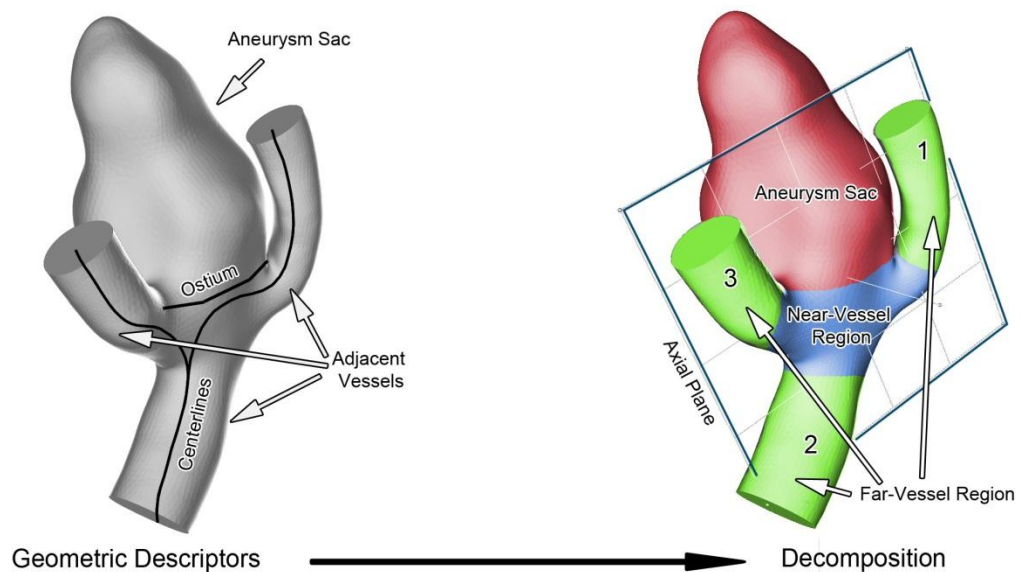

Fig. 2 *The surface mesh, centerlines and the ostium plane are employed to decompose the surface and calculate the axial plane*

The overall shape of an aneurysm sac is convex while cross sections of the adjacent vessels normally exhibit a cylindrical shape (see Figure 2). However, this shape significantly deviates close to the aneurysm. We define the far-vessel-regions as regions, where vessel cross sections are cylindrical while the near-vessel-region contains the variably formed vessel area below the aneurysm. This definition can be seen as a stricter, geometry-driven interpretation of the near- and

5

far-parent vessel definition of Cebral and Shojima [14]. They define far- and near-vessel regions depending on the distance being above or below *1.0 cm* to the aneurysms ostium respectively. Additionally, our analysis approach does not distinguish between the parent vessel of the aneurysm and other vessels at bifurcations; they are all referred to as adjacent vessels.

When excluding the aneurysm sac, the adjacent vessels exhibit a planar layout, at least close to the aneurysm. The axial plane is an abstract descriptor for this planar layout. Roughly described, this plane cuts the dataset in half, defining two subspaces that directly relate to the underlying vessel configuration. Those subspaces and the normal vector of the plane are helpful descriptors for various geometric tasks. Two of which, are described later on: viewpoint selection and the definition of a vessel order.

Reconstruction Pipeline

The image data is obtained from CTA or MR-ToF. The vessel lumen is contrast-enhanced either through application of a contrast agent or, in case of MR-ToF, by usage of the Time-of-Flight sequence. Due to the enhanced vessel contrast, we are able to employ thresholding for segmentation. In most cases the spatial resolution is sufficiently high and the partial volume effect has only minor influence on the reconstruction quality. However, if the signal-to-noise ratio is low or the vessel lumen is not sufficiently represented, for instance in the case of incomplete distribution of the contrast agent, model-based segmentation [15] is used.

However, the accuracy of the resulting segmentation is influenced by various parameters like image modality, scanning parameters, motion artifacts, or parameterization of the segmentation algorithm. An in-depth discussion of this influence is beyond the scope of this paper. For further reading we refer to [16], who present a comparative study on segmentation of 3DRA and MRA datasets, [17], who evaluate the influence of segmentation on flow analysis and [15], who give an overview of 3D vessel lumen segmentation. The segmentation results of the datasets presented in this publication were evaluated by a board certified neuroradiologist.

The dilated (3x3 kernel) binary segmentation mask is applied to the original dataset. The masked dataset forms the input to the *Marching Cubes* algorithm.

Using the same intensity value as for thresholding, we obtain a triangulated surface representation that encloses the vessel lumen as output.

Depending on the application (visualization, CFD, etc.) and the quality of the image data, several post-processing steps might be necessary. They include the removal of surface noise, orthogonal cutting of in- and outlets or the removal of vessel blending, caused by partial volume effects during segmentation. A detailed description of the post-processing pipeline is given in [18]. Once the shape quality of the surface is sufficient, the quality of the surface triangles is improved by means of an advancing front remeshing [19].

Ostium and Centerline Calculation

For the surface decomposition, two additional geometric descriptors need to be derived from the surface: the centerlines of the adjacent vessel and the ostium plane. For the calculation of the centerlines, we employ VMTK. The only user interaction is the selection of the start- and endpoint of each centerline. A 3D Voronoi diagram is calculated from the surface mesh and used to define the centerline. This is a robust approach and since the resulting centerlines are directly derived from the polygonal surface, they are suitable as geometric paths for subsequent surface sampling. For details on the calculation of the centerlines we refer to [6]. To generate the ostium plane, we employ an iterative approach presented in [10]. The surface, centerlines and one user-defined point on the aneurysm sac are needed as input and the output are four control points, placed between adjacent vessels and the aneurysm sac. A specific interpolation scheme [20] is used to generate a bent, smooth surface from the control points. This surface represents the ostium plane. By cutting the surface mesh with the ostium plane, an initial decomposition between the adjacent vessels and the aneurysm is given. In the next step the adjacent vessels are decomposed into near- and far-vessel regions.

Adjacent Vessel Analysis

The two main mechanisms of our decomposition approach are based on approximation: approximation of the vessel's cross section shape and approximation of the vessel area profile along the centerline. Both are based on

sampling the vessels along their centerlines. For each adjacent vessel, the sampling starts at the in/outlets and is performed towards the aneurysm.

Cross Section Shape Approximation: The centerline is represented by a set of connected vertices. Three successive centerline vertices p_1, p_2 and p_3 are used to compute the normal vector $\vec{n} = (\overrightarrow{p_1 p_2} + \overrightarrow{p_2 p_3})/2$ of an orthogonal cutting plane whereas p_2 is the plane's origin. When cutting the polygonal mesh with this plane, we obtain sets of vertices. The set closest to the centerline represent the cross section of the current centerline's vessel. We approximate this cross section by an ellipse. This has two advantages: increased robustness against surface noise and a local coordinate system given by the minor- and major axis of the ellipse.

To compute the approximation ellipse, we interpret the vertices of the cross section set as multivariate random variables and compute their covariance matrix. The eigenvectors scaled by the eigenvalues represent the minor and major axis of the approximation ellipse. To reduce computation complexity, we decrease the dimensionality from 3D to 2D by using the tangential space of the plane as the computation domain, leading to a 2x2 covariance matrix. Figure 3 shows an overview of the cross section approximation.
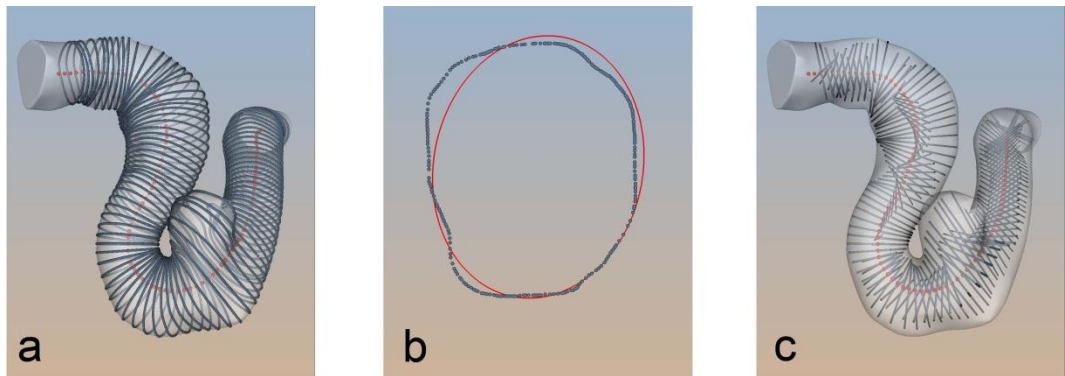

Fig. 3 *Surface sampling along the centerline (a), the approximation ellipse (red) of one selected set of cut vertices in the 2D domain (b) and the minor/major axes of the approximation ellipses mapped back into the 3D domain*

Vessel Area Profile Approximation: Once the approximation ellipses for all centerline positions are computed, we employ the area $A = \pi a b$, whereas a and b are the lengths of the major and minor axis, of each ellipse to generate an area profile over the complete centerline. An exemplarily profile is shown in Figure 4.
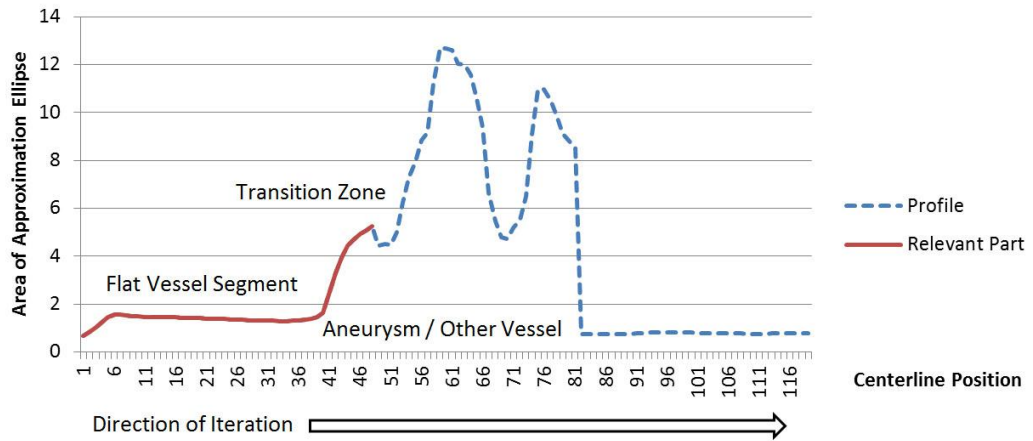
Fig. 4 *Example of a vessel area profile: the relevant part includes the flat vessel segment and the transition zone*

We iterate over this profile, from in/outlet towards the aneurysm. It first exhibits a more or less flat segment with rather small changes of *A*. This data segment represents the far-vessel region of the current adjacent vessel. A significant increase of the profile values indicates that the underlying centerline has left the vessel, now sampling areas within the aneurysm or neighbouring vessels. This transition zone, from rather flat profile segments to segments with high, rapidly changing values marks the transition from far- to near-vessel region. However, the identification of the exact location of this transition zone is not trivial, due to surface noise and a high anatomic variability (e.g. variance of the vessel diameter, neck-to-dome ratio, ratio of vessel diameter and aneurysm size). Thus, we identify the relevant part of the profile and approximate this segment with an analytical model function (see Figure 5). On this model function we can robustly identify the transition zone by means of curve analysis.
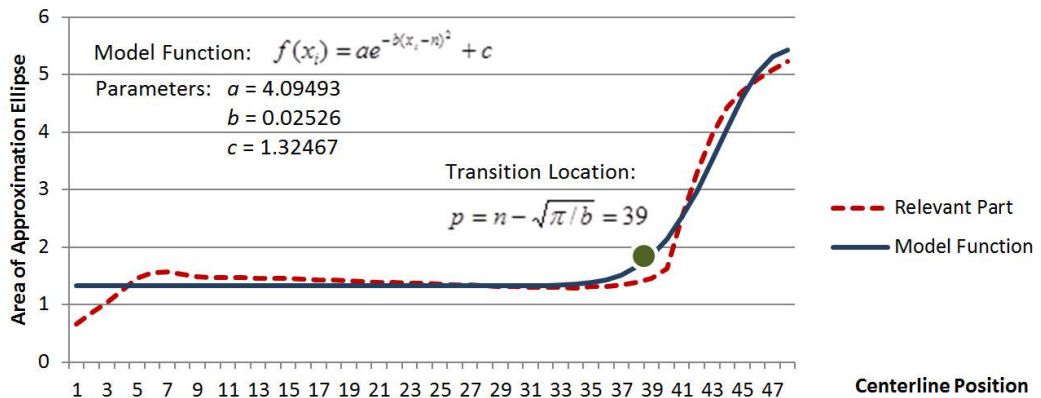

Model Function: $f(x_i) = ae^{-b(x_i-n)^2} + c$

Parameters: $a = 4.09493$
$b = 0.02526$
$c = 1.32467$

Transition Location:

$p = n - \sqrt{\pi/b} = 39$

9

Fig. 5 *Example result of the Levenberg-Marquardt algorithm, the transition location can be directly derived from the parameters of the fitted Gaussian function*

The relevant part of the profile only includes the flat vessel segment and the first increase peak, marking that areas outside the current vessel were sampled. We exclude the rest of the profile. It only includes the vessel area profile of other adjacent vessels and a more or less arbitrary sampling of areas within the aneurysm.

We employ the first half of the symmetric Gaussian function $f(x_i) = ae^{-b(x_i-n)^2} + c$ as model function, since its shape resembles the flat vessel segment with the follow-up peak. The function parameter a, b and c control height, width and shift of the Gaussian curve, whereas x_i represent the current of the n positions of the relevant profile part.

Matching this model function to the profile is a least squares curve fitting problem. It can be efficiently solved with the Levenberg-Marquardt algorithm, which interpolates between the Gauss-Newton algorithm and the gradient descent method. It uses the profile values and the Gaussian function as input and iteratively alters the three function parameters a,b and c until the squared distance between profile and function values is minimized. Once the model function is parameterized, we can derive the transition location p with $p = n - \sqrt{\pi/b} = 39$, which is derived from the variance of the generalized Gaussian curve.

To address the local profile variability at the transition zones that is not resembled by our model function, we can optimize the found transition location through local comparison of model function and profile. If the profile value at the transition location exceeds the value of the model function, we iterate backwards ("away from the aneurysm") until the model function value is higher than the profile value. An analogous forward transition is performed if the profile value exceeds the model function value. These two local optimization mechanisms can be optionally applied, as the initially found transition zone location might not be sufficient in some cases. Thus, we provide a simple, parameter-free correction option to the user.

Axial Plane: Calculation and Applications

The transition locations in the profiles of all adjacent vessels can be directly mapped to a position on their centerlines. They form the center points p_i of the orthogonal circular transition zones that separate the near- from the far-vessel regions (see Figure 6). We include the ostium center point, the average of all positions of the ostium contour, to this point set. The points are used to estimate the position and orientation of the axial center plane. A robust approach for this is to calculate the best-fit plane [21]. The calculation of the best-fit plane is an optimization problem. For the center points $p_1, ..., p_m$ we have to find an optimal plane $n_1x + n_2y + n_3z + d = 0$ which minimizes the sum of the squared distances of the center points and the plane. Our minimization problem is

$$\min_{n,d} \sum_{i=0}^{m} \frac{\left(\langle n, p_i \rangle + d\right)^2}{\langle n, n \rangle}$$

When considering the matrix $P^T = (p_0 - p_c \quad ... \quad p_m - p_c)$ the optimization problem changes to:

$$\min_{n,d} \frac{n^T P^T P n}{\langle n, n \rangle}$$

This quotient is called the *Rayleigh-Quotient*. It reaches its minimum value when n is the eigenvector of $P^T P$ with corresponding minimal eigenvalue. Thus, the minimization problem reduces to an eigenvector problem. After determining the lowest eigenvalue λ we have to find a non-zero vector v fulfilling the equation $(P^T P - \lambda I)v = 0$, where I is the identity matrix.

The plane parameters given by vector v describe a plane that is as close as possible to all center points. Thus, it is oriented in a way that, at least close to the aneurysm, it cuts all adjacent vessels as well as the aneurysm sac. This anatomy-driven orientation enables a number of geometric applications, two of which are described in the following.

Adjacent Vessel Ordering: The definition of a unique vessel order, and derivable data like size deviation or angle between neighboring vessels, is a high level description of the dataset. This kind of data is necessary to tag, identify and compare datasets that are stored in a medical research database.

We employ the axial plane to reduce the problem from the in some cases ambiguous 3D domain to the 2D domain. The center points p_i of each transition

zone and the ostium center point p_o are projected into the plane space (see Fig. 4). The plane space projection of p_o marks the unique starting point for the consecutive numbering of the vessels.
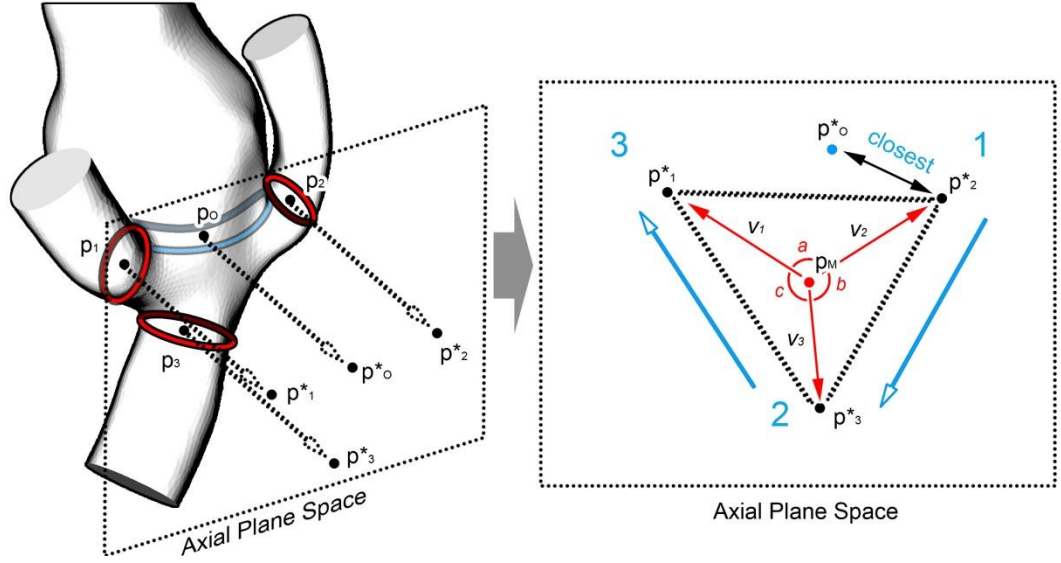

Fig. 6 *The center points p_i are calculated from the transition zones (red) and the ostium contour (blue) and projected into plane space. There the planar center point p_M is used to define an order via angle (a,b,c) comparison.*

The projected center point p^*_i closest to the projected ostium center point p^*_o is the starting point $p_{current}$ for the ordering process and the *ID 1* is assigned to it. A planar center point p_M is calculated by averaging the projected center point coordinates. Additionally, for each p^*_i, a vector $v_i = \overrightarrow{p_M p^*_i}$ is defined. The ordering is an iterative process. The vector angles between $V_{current}$ and the vectors v_i of all unprocessed projected points p^*_i are calculated. The point with the smallest vector angle will be $p_{current}$ for the next iteration. It is marked as processed and an *ID* increased by one is assigned to it. Since we also want to define a unique ordering direction, we add an additional constraint to the first iteration. Besides having the smallest vector angle, the next point also has to point "away" from the projected ostium center point p^*_o with respect to $p_{current}$. This is done by comparing the directions of the cross-product vectors $c_{current} = \overrightarrow{p_M p_o} \times \overrightarrow{p_M p_{current}}$ and $c_i = \overrightarrow{p_M p_o} \times \overrightarrow{p_M p^*_i}$. If $c_{current}$ and c_i point in the same direction, p^*_i is valid. If not, the remaining projected points are checked, sorted by ascending vector angles, until a valid point is found. When all projected

points are processed, the assigned IDs define a unique order of the adjacent vessels in the near-vessel region.

This unique order is a basic layout that can be supplemented with additional data, depending on the further application. For example, if flow data is present, the starting point can be defined at the inflow vessel through a simple shift of the given order. The parent vessel can also be derived, since it is represented by the adjacent vessels left and right of the ostium, thus, the adjacent vessels with the second lowest and highest ID.

Viewpoint Selection: Exploration of multi-dimensional data while navigating three-dimensional space can be a tedious task. A well-chosen initial viewpoint can help to gain a spatial overview of the given data. It also serves as start position for the exploration process the user can go back to, once a specific exploration step is completed. In field of 3D interaction, viewpoint selection is an established technique to support the exploration process [22].

A suitable initial viewpoint can be defined as a viewpoint that provides a minimal grade of visual occlusion (e.g. the adjacent vessels might occlude the aneurysm sac). The axial plane is oriented such that it minimizes the distance to the center points of ostium contour and adjacent vessel transition zones. Thus, its normal vector automatically provides a view towards the "side" of the set of center points, minimizing the chance of occlusion (see Figure 10). The viewpoint selection should also reflect that the aneurysm sac is the main feature of interest. This is achieved by using the inverted plane normal as viewing direction, if most of the aneurysm sac vertices are on the opposing side of the axial plane.

Results

We applied our approach to 9 datasets from the MOBESTAN database (project funded by Saxony-Anhalt – Germany - 5161AD/0308M, contact: preim@isg.cs.uni-magdeburg.de). The chosen datasets represent the anatomic variability of cerebral aneurysms, including small, medium and big side aneurysms and small to giant bifurcation aneurysms with up to 6 adjacent vessels. On all datasets, decomposition could be automatically achieved (see Figure 7). No user interaction was necessary to create these results and the computation time for one transition zone ranged within one to three seconds on a standard desktop pc (Intel Core 2 Duo 3 GHz, 4 GB RAM).
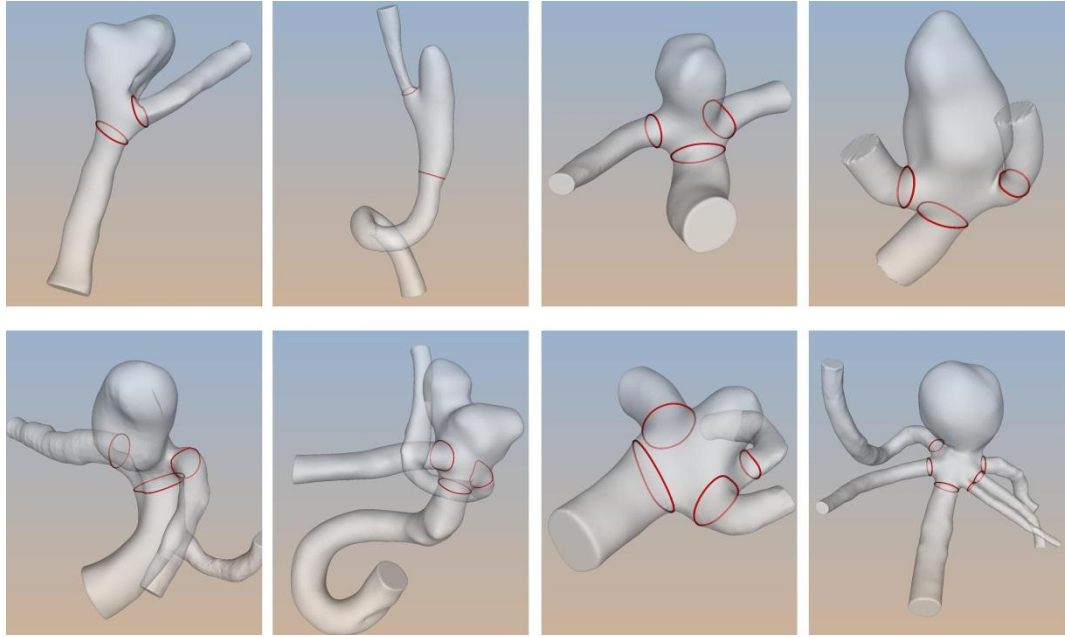
Fig. 7 *Results of the automatic decomposition: the transition zones (red) separate near- and far vessel regions, the datasets exhibit increasing anatomic complexity, from a side-wall aneurysm (top left) to a giant bifurcation aneurysm (bottom right) with 6 adjacent vessels*

To evaluate the robustness of the decomposition, artificial random noise was added to all surface meshes, simulating local surface variability and suboptimal reconstruction results (see Figure 8). With a noise level that randomly alters the local surface diameter up to 15% our approach could be successfully applied to all datasets. Six out of the nine datasets could be successfully decomposed with a noise level of up to 30%.
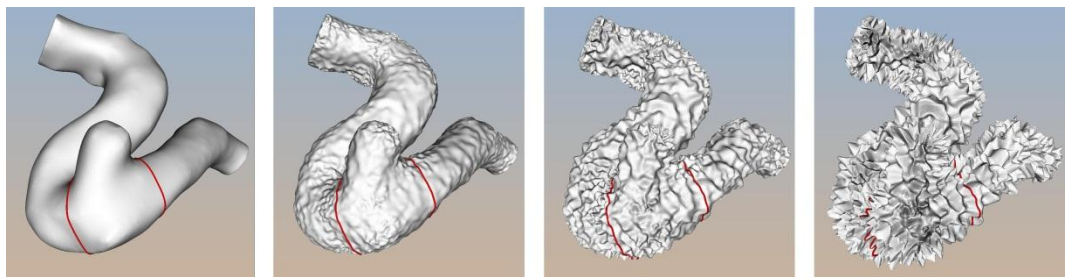

Fig. 8 *Results of the automatic decomposition at different noise levels (left to right): 0%, 5%, 15%, 30%*

To evaluate the correctness of the decomposition, we performed a questionnaire with four medical experts, two of which are board certified neuroradiologists. The experts were asked to manually draw the transition zones on all datasets. Then the

14

averaged results have been qualitatively compared with the results of our automatic approach. The manual and automatic results showed a sufficient conformity for most of the transition zones (center point locations deviation < 10% vessel diameter), however, in some cases there was a significant deviation (see Figure 9).
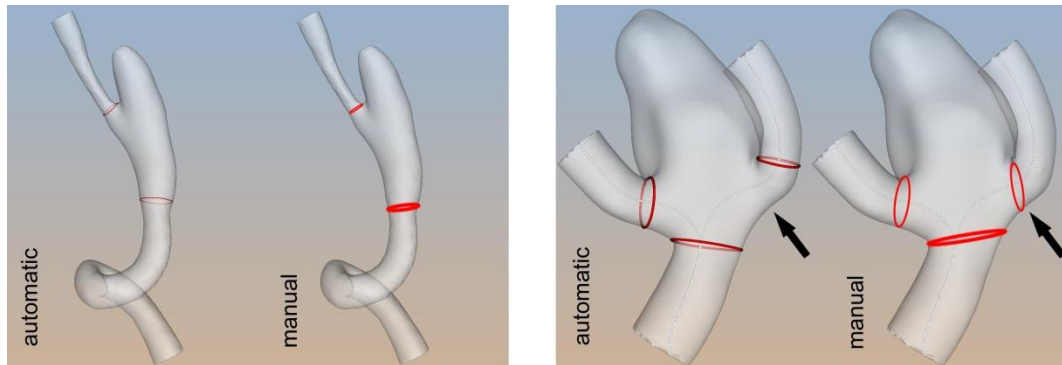

Fig. 9 *Comparison of automatic and manual (ring thickness represents variance of data) decomposition exhibits good conformity in most cases (left image), in some case a characteristic deviation could be observed (arrow)*

To gain additional qualitative feedback, an informal interview with one of the neuroradiologists was carried out. He is currently involved in a project that focuses on the relation between complex time dependent flow patterns and the location of an aneurysm rupture. He confirmed the need for additional geometric descriptors besides ostium contour and centerlines and stated that the transition zones are useful for tasks like seeding streamlines and masking parts of the flow field. He also confirmed the benefit of automatic viewpoint selection to support the navigation. The viewpoints provided by our approach (see Figure 10) were considered to be good starting positions for an initial overview and further exploration.
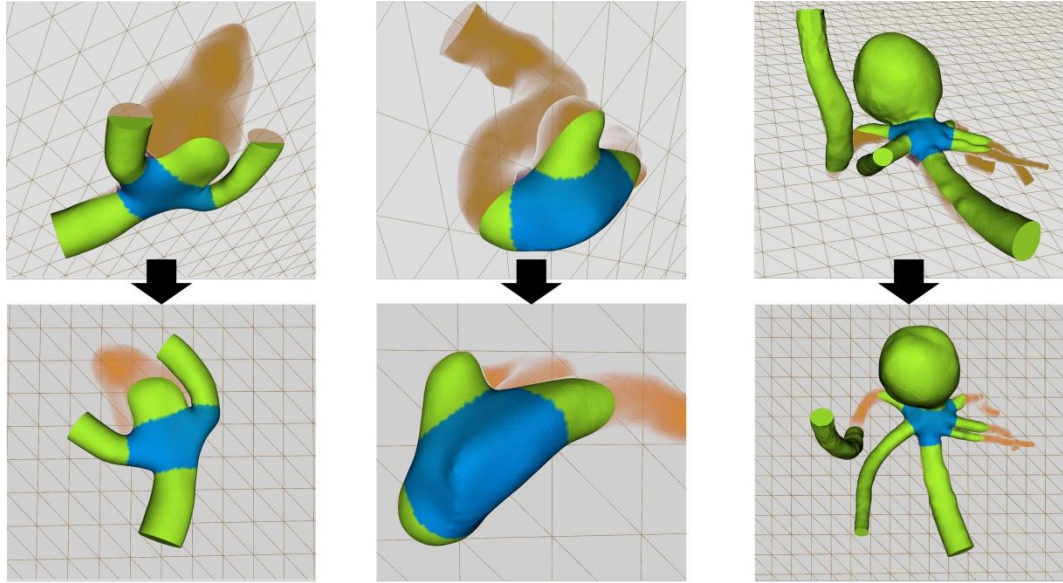
Fig. 10 *Examples for automatic viewpoint selection: the normal vector of the axial plane (transparent mesh) is used as viewing direction (bottom row)*

Discussion

Since our automatic decomposition approach is robust even against severe surface noise, it provides sufficient results in all tested cases. This robustness is mainly attributable to the approximation of the vessel area and the area profile by means of model functions. Thus, our approach is also suitable for data with lower quality, as it may result from suboptimal scanning conditions or a simplified reconstruction pipeline.

However, the vessel area profile must still contain the expected basic layout: a more or less flat segment (areas sampled within the vessel) followed by a peak (areas sampled within the aneurysm/other vessels). In case of a deformed vessel with strong local diameter changes, these changes could be misinterpreted as aneurysms. This would result in a transition zone located close to the diameter change rather than close to the aneurysm. If the aneurysm is very small (e.g. < 30% of vessel diameter) and if it has no distinct neck, it might not be represented strong enough in the area profile, also leading to misplaced transition zones.

A solution, at least for the first case, could be the iterative provision of all potential transition zones. The start of the vessel area profile would need to be shifted to the location of the last found transition zone, followed by a rerun of the analysis process until the end of the centerline is reached. The user could choose

the correct transition zone from the resulting set. However, for cases with small, underrepresented aneurysms a manual decomposition would be necessary.

The evaluation of the correctness has shown sufficient comparability for most of the transition zones. However, in some cases, the manual selection of all experts characteristically deviated from the results of the automatic approach. We were able to identify the orthogonal sampling of the vessel profile as cause for the deviation. The automatically generated transition zones are always orthogonal with respect to the centerline. The manually selected transition zones tend to mark the non-orthogonal end of the vessel. Both definitions are meaningful: while the automatic selected orthogonal transition zones are suitable for probing flow characteristics (e.g. volumetric flow), the manual selected transition zones are closer to the anatomic layout. It could be observed that both kinds of transition zones share one coincident point and the deviation can be described as a rotation around this point.

We provide a simple-to-use widget for manual correction (see Figure 11). The minor/major axes of the approximation ellipses provide us with a local coordinate system for the widget. The end-points of each axis are used as handles. Dragging one handle leads to a rotation around the opposing handle. After rotation, the cut is updated to generate a new transition zone contour. Thus, one can align the automatic with the manual transition zone with just one dragging operation. Yet we recommend keeping the automatic generated transition zones, if the further application involves any kind of flow probing.
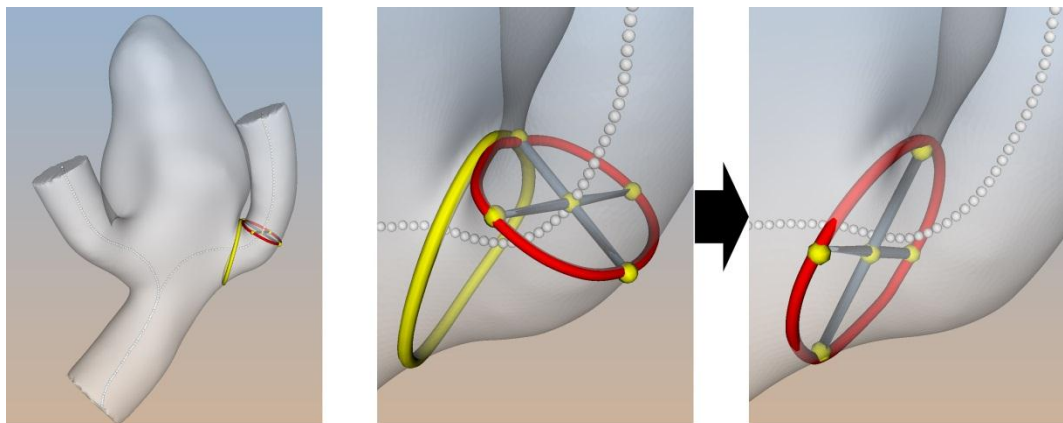

Fig. 10 *Widget for correction: dragging a handle (yellow sphere) rotates the transition zone around the opposing handle, for this, the local coordinate system (grey tubes) is employed (yellow ring – manual selected transition zone)*

Conclusion

We presented an approach that automatically decomposes vessels adjacent to an aneurysm into near- and far-vessel regions. The transition zones that separate near-vessel from far-vessel regions were used to calculate a characteristic axial plane. We presented two applications for this multi-purpose plane: automatic vessel order calculation and automatic viewpoint selection. The decomposition was successfully applied to datasets with high anatomic variability and a comparison with results that were manually created by experts showed a good conformance. Cases of non-conformance exhibited a characteristic layout and we provided a specialized widget to reproduce the manual solution.

The automatic computation of the anatomic descriptors is a valuable extension to existing exploration workflows and research database applications. Future work will concentrate on the integration process and focus on additional application dependent requirements that may arise.

References

[1]   PARLEA L., FAHRIGA R., HOLDSWORTH D.W., LOWNIEA S.P.: An Analysis of the Geometry of Saccular Intracranial Aneurysms. Neuroradiology (1999) 20:1079-1089

[2]   CEBRAL R., CASTRO M.A., BURGESS J.E., ET AL: Characterization of Cerebral Aneurysms for Assessing Risk of Rupture by Using Patient-Specific Computational Hemodynamics Models. Neuroradiology (2005), 26:2550-2559

[3]   SESHADHRI S., GABOR J., BEUING O., SKALEJ M., THEVENIN D.: Impact of Stents and Flow Diverters on Hemodynamics in Idealized Aneurysm Models. Biomechanical Engineering (2011) 133:071005

[4]   LARRABIDE I, OMEDAS P., MARTELLI Y., ET AL: GIMIAS: an open source framework for efficient development of research tools and clinical prototypes. Functional Imaging and Modelling of the Heart (2009) 5528:417-426

[5]   KUHN A., LEHMANN D.J., GASTSTEIGER R., ET AL: A Clustering-based Visualization Technique to Emphasize Meaningful Regions of Vector Fields VMV (2011) 191-198

[6]   ANTIGA L., PICCINELLI M., BOTTI L., ET AL.: An Image-Based Modelling Framework for Patient-Specific Computational Hemodynamics. Medical and Biological Engineering and Computing (2008), 46:1097-1112

[7]   PICCINELLI, M. AND VENEZIANI, A. AND STEINMAN, D.A., ET AL.: A Framework for Geometric Analysis of Vascular Structures: Application to Cerebral Aneurysms. Trans. On Medical Imaging, 28:1141-1155

[8]   MA B., HARBAUGH R.E., RAGHAVAN M.L.: Three-Dimensional Geometrical Characterization of Cerebral Aneurysms. Annals of Biomedical Engineering (2004), 32: 264-273

[9]   SGOURITSA, E., MOHAMED, A., MORSI, H. ET AL.: Neck Localization and Geometry Quantification of Intracranial Aneurysms. Proc. of IEEE Biomedical Imaging (2010), 1057-1060

[10]   NEUGEBAUER M., DIEHL V., SKALEJ M., PREIM B.: Geometric Reconstruction of the Ostium of Cerebral Aneurysms. Proc. of Vision, Modeling, Visualization (2010), 307-314

[11]   TATESHIMA S., CHIEN A., SAYRE J., ET AL.: The Effect of Aneurysm Geometry on the Intra-Aneurysmal Flow Conditions. Neuroradiology (2010) 52:1135–114

[12]   MANTHA A., BENNDORF G., HERNANDEZ A., METCALFE R.: Stability of Pulsatile Blood Flow at the Ostium of Cerebral Aneurysms. Journal of Biomechanics (2009), 42:1081-1087

[13]   BAHAROGLU M., SCHIRMER C., HOIT D., ET AL.: Aneurysm Inflow-Angle as a Discriminant for Rupture in Sidewall Cerebral Aneurysms: Morphometric and Computational Fluid Dynamic Analysis. Stroke (2010), 7:1423-1430

[14]   CEBRAL J.R., MUTA F., WEIR J., PUTMAN C.: Quantitative Characterization of the Hemodynamic Environment in Ruptured and Unruptured Brain Aneurysms. Neuroradiology (2011) 32:145-151

[15]   LESAGE D., ANGELINI E. D., BLOCH I., FUNKA-LEA G.: A review of 3D vessel lumen segmentation techniques: Models, features and extraction schemes. Medical Image Analysis (2009), 13:819–845

[16]   BOGUNOVIC H., POZO J.M., VILLA-URIOL M.C., ET AL: Automated segmentation of cerebral vasculature with aneurysms in 3DRA and TOF-MRA using geodesic active regions: an evaluation study. Medical Physics (2011) 38:210-219

[17]   SEN Y., QIAN, Y., ZHANG, Y., MORGAN, M.: A comparison of medical image segmentation methods for cerebral aneurysm computational hemodynamics. BMEI (2011) 2:901-904

[18]   MÖNCH T., NEUGEBAUER M., PREIM B.: Optimization of Vascular Surface Models for Computational Fluid Dynamics and Rapid Prototyping. Second International Workshop on Digital Engineering (2011), 16-23

[19]   SCHÖBERL J.: NETGEN: An advancing front 2D/3D mesh generator based on abstract rules. Computing and Visualization in Science (1997), 1: 41–52

[20]   NEUGEBAUER M., PREIM B.: Generation of a Smooth Ostium Surface for Aneurysm Surface Models. Proc. of BVM (2011), 399-403

[21]   FORBES A.: Least squares best-fit geometric elements. Algorithms for approximation (1990), 1988: 311

[22]   MÜHLER K., NEUGEBAUER M., TIETJEN C., PREIM, B: Viewpoint selection for intervention planning. EuroVis (2007) 267-274